Geochimica et Cosmochimica Acta, Vol. 69, No. 7, pp. 1873–1881, 2005

0016-7037/05 $30.00 + .00

doi:10.1016/j.gca.2004.06.046

Origin of low-Ca pyroxene in amoeboid olivine aggregates: Evidence from oxygen isotopic compositions

ALEXANDER N. KROT,[1,*] TIMOTHY J. FAGAN,[2,†] KAZUHIDE NAGASHIMA,[2] MICHAEL I. PETAEV,[3] and HISAYOSHI YURIMOTO[2]

[1]Hawaií Institute of Geophysics and Planetology, School of Ocean and Earth Science and Technology, University of Hawai'i at Manoa, Honolulu, HI 96822, USA

[2]Department of Earth and Planetary Sciences, Tokyo Institute of Technology, Tokyo 152-8551, Japan

[3]Harvard-Smithsonian Center for Astrophysics and Department of Earth and Planetary Sciences, Harvard University, Cambridge, MA 02138, USA

(*Received December* 9, 2003; *accepted in revised form June* 7, 2004)

Abstract—Amoeboid olivine aggregates (AOAs) in primitive carbonaceous chondrites consist of forsterite ($Fa_{<2}$), Fe,Ni-metal, spinel, Al-diopside, anorthite, and rare gehlenitic melilite ($Åk_{<15}$). ~10% of AOAs contain low-Ca pyroxene ($Fs_{1-3}Wo_{1-5}$) that is in corrosion relationship with forsterite and is found in three major textural occurrences: (*i*) thin (<15 μm) discontinuous layers around forsterite grains or along forsterite grain boundaries in AOA peripheries; (*ii*) 5–10-μm-thick haloes and subhedral grains around Fe,Ni-metal nodules in AOA peripheries, and (*iii*) shells of variable thickness (up to 70 μm), commonly with abundant tiny (3–5 μm) inclusions of Fe,Ni-metal grains, around AOAs. AOAs with the low-Ca pyroxene shells are compact and contain euhedral grains of Al-diopside surrounded by anorthite, suggesting small (10%–20%) degree of melting. AOAs with other textural occurrences of low-Ca pyroxene are rather porous. Forsterite grains in AOAs with low-Ca pyroxene have generally ^{16}O-rich isotopic compositions ($\Delta^{17}O < -20‰$). Low-Ca pyroxenes of the textural occurrences (*i*) and (*ii*) are ^{16}O-enriched ($\Delta^{17}O < -20‰$), whereas those of (*iii*) are ^{16}O-depleted ($\Delta^{17}O = -6‰$ to $-4‰$). One of the extensively melted (>50%) objects is texturally and mineralogically intermediate between AOAs and Al-rich chondrules. It consists of euhedral forsterite grains, pigeonite, augite, anorthitic mesostasis, abundant anhedral spinel grains, and minor Fe,Ni-metal; it is surrounded by a coarse-grained igneous rim largely composed of low-Ca pyroxene with abundant Fe,Ni-metal-sulfide nodules. The mineralogical observations suggest that only spinel grains in this igneous object were not melted. The spinel is ^{16}O-rich ($\Delta^{17}O \sim -22‰$), whereas the neighboring plagioclase mesostasis is ^{16}O-depleted ($\Delta^{17}O \sim -11‰$).

We conclude that AOAs are aggregates of solar nebular condensates (forsterite, Fe,Ni-metal, and CAIs composed of Al-diopside, anorthite, spinel, and ±melilite) formed in an ^{16}O-rich gaseous reservoir, probably CAI-forming region(s). Solid or incipiently melted forsterite in some AOAs reacted with gaseous SiO in the same nebular region to form low-Ca pyroxene. Some other AOAs appear to have accreted ^{16}O-poor pyroxene-normative dust and experienced varying degrees of melting, most likely in chondrule-forming region(s). The most extensively melted AOAs experienced oxygen isotope exchange with ^{16}O-poor nebular gas and may have been transformed into chondrules. The original ^{16}O-rich signature of the precursor materials of such chondrules is preserved only in incompletely melted grains.

1. INTRODUCTION

Amoeboid olivine aggregates in primitive (unmetamorphosed and unaltered) carbonaceous chondrites consist of forsteritic olivine ($Fa_{<2}$), Fe,Ni-metal, and a refractory component (fine-grained minerals, either assembled into individual CAIs or interspersed with forsterite grains) composed of Al-diopside, spinel, ±anorthite, and ±melilite; secondary iron- and alkali-rich minerals, commonly observed in the oxidized CV chondrites (Grossman and Steele, 1976; McSween, 1977; Cohen et al., 1983; Kornacki and Wood, 1984a,b; Hashimoto and Grossman, 1987) and metamorphosed CO chondrites (e.g., Chizmadia et al., 2002), are absent (Komatsu et al., 2001; Itoh et al., 2002; Krot et al., 2004a,b,c). Approximately 10% of more than 500 AOAs studied by Krot et al. (2004a) in the CR, CV, CM, CO, CH, CB, and ungrouped carbonaceous chondrites Acfer 094, Adelaide, and Lewis Cliff (LEW) 85332 contain low-Ca pyroxene replacing forsterite. Three major textural occurrences of low-Ca pyroxene in AOAs were identified: (*i*) thin (<15 μm) discontinuous layers around forsterite grains or along forsterite grain boundaries in AOA peripheries; (*ii*) 5–10-μm-thick haloes and subhedral grains around Fe,Ni-metal nodules in AOA peripheries, and (*iii*) shells of variable thickness (up to 70 μm), commonly with abundant tiny (3–5 μm) inclusions of Fe,Ni-metal grains, around AOAs. Some of the AOAs with low-Ca pyroxene (px-AOAs) appear to have experienced varying degrees of melting. In the most extensively melted AOAs, classified as AOA/chondrule-like objects, only spinel grains appear to have escaped melting.

Based on these observations, Krot et al. (2004a) concluded that the first two occurrences of low-Ca pyroxene formed by reaction between forsterite and gaseous SiO, possibly in CAI-forming region(s). The low-Ca pyroxene shells around AOAs might have formed by direct gas-solid condensation from fractionated (Mg/Si ratio < solar) nebular gas or by accretion of pyroxene-normative dust around AOAs followed by subse-

* Author to whom correspondence should be addressed (sasha@higp.hawaii.edu).

† *Present address:* Smithsonian Institution, Department of Mineral Sciences, NHB 119, Washington DC 20560, USA.

Table 1. Electron microprobe analyses of low-Ca pyroxenes, sub-Ca pyroxenes, and olivines in AOAs and in an AOA-like object in carbonaceous chondrites.[a]

Chondrite AOA #	Acfer 094			PCA91082			NWA 1180		Murchison		Leoville			
ox/mineral	105 px	105 ol	24 px	24 ol	35 px	35 ol	10 px	10 ol	32 px	32 ol	1 px	1 cpx	1 ol	1 ol
SiO_2	55.9	42.3	59.4	42.3	57.5	42.5	58.11	42.3	56.7	42.8	57.3	55.6	42.4	41.9
TiO_2	0.22	0.12	<0.09	0.12	0.17	<0.09	0.27	<0.09	0.52	<0.09	0.66	0.67	<0.09	0.12
Al_2O_3	0.25	0.04	0.58	0.16	2.0	0.05	0.38	0.05	1.1	<0.03	1.6	1.7	<0.03	<0.03
Cr_2O_3	0.30	0.25	0.27	0.17	0.84	0.52	0.19	0.19	0.67	0.44	0.56	0.62	0.12	0.17
FeO	0.78	0.39	0.81	0.35	1.8	1.2	1.0	0.81	1.6	1.3	0.57	0.96	0.89	2.5
MnO	<0.07	0.09	0.09	<0.07	0.37	0.32	<0.07	0.16	0.29	0.57	0.07	0.12	0.09	0.12
MgO	38.7	57.1	39.6	56.5	35.6	56.2	39.7	57.2	38.3	56.6	38.4	32.2	56.9	55.9
CaO	0.74	0.10	0.60	0.19	2.6	0.22	0.82	0.10	2.4	0.19	0.76	7.4	0.17	0.17
Na_2O	<0.06	<0.06	<0.06	<0.06	<0.06	<0.06	<0.06	<0.06	<0.06	<0.06	<0.06	<0.06	<0.06	<0.06
K_2O	<0.04	<0.04	<0.04	<0.04	<0.04	<0.04	<0.04	<0.04	<0.04	<0.04	<0.04	<0.04	<0.04	<0.04
total	96.9	100.5	101.4	99.9	100.9	101.0	100.6	100.9	101.5	101.8	99.9	99.3	100.6	100.9
Fa, mol%	—	0.4	—	0.4	—	1.1	—	0.8	—	1.2	—	—	0.9	2.4
Fs, mol%	1.1	—	1.1	—	2.7	—	1.4	—	2.2	—	0.8	1.4	—	—
Wo, mol%	1.3	—	1.1	—	4.9	—	1.4	—	4.2	—	1.4	13.9	—	—

[a] ox = oxide (wt%); ol = olivine; px = low-Ca pyroxene; cpx = sub-Ca pyroxene.

quent melting, possibly during chondrule formation. Because CAIs in most carbonaceous chondrites originated in an ^{16}O-rich gaseous reservoir (Aléon et al., 2002a; Krot et al., 2002a), whereas chondrules appear to have formed in the presence of ^{16}O-poor gas (e.g., Leshin et al., 2000), this hypothesis can be tested by studying O-isotopic compositions of low-Ca pyroxenes in AOAs. If low-Ca pyroxenes originated in chondrule-forming region(s), they are expected to be systematically ^{16}O-depleted relative to forsterite.

Here, we report O-isotopic compositions of five px-AOAs and one AOA/Al-rich chondrule-like object described in detail by Krot et al. (2004a), and discuss their significance for understanding the origins of low-Ca pyroxene in AOAs and possible implications for chondrule formation.

2. SAMPLES AND ANALYTICAL TECHNIQUES

Polished sections of Acfer 094, Adelaide, and LEW85332 and meteorites from the CR, CB, CH, CM, CV, and CO groups were X-ray mapped in Ca, Al, Mg, Si, Cr, Ni, Mn, Ti, and Na Kα with resolution of 5–10 μm (2 μm for individual AOAs) with a Cameca SX50 electron microprobe, and in Ca, Al, Mg, Si and Fe Kα with 0.3 μm probe steps with a JEOL 5310LV scanning electron microscope (SEM) + Oxford LINK ISIS energy dispersive electron microprobe system. The identified AOAs were studied in backscattered electron (BSE) mode with a JEOL 5900LV SEM. Mineral compositions were determined with the Cameca SX50 electron microprobe using 15 KeV accelerating voltage, 10–20 nA (for silicates) and 30 nA (for metal) current, a focused (~1–2 μm) beam, and well-characterized silicate, oxide, and metal standards. For each element, counting times on both peak and background were 30 s (10 s for Na and K; Na and K were analyzed first). Matrix corrections were applied using a PAP software routine. The element detection limits for silicates are (in wt%) SiO_2, Al_2O_3, MgO, 0.03; TiO_2, CaO, K_2O, 0.04; Na_2O, Cr_2O_3, 0.06; MnO, 0.07; FeO, 0.08.

Five AOAs showing the range of textural occurrences of low-Ca pyroxene identified previously (Krot et al., 2004a) were selected for O-isotopic analysis. The AOAs are from two CR chondrites [Pecora Escarpment (PCA) 91082 and Northwest Africa (NWA) 1180], an unclassified carbonaceous chondrite (Acfer 094) and a CM chondrite (Murchison). The two CR chondrites and Acfer 094 have undergone minimal, if any, aqueous alteration or thermal metamorphism. In contrast, Murchison has experienced some aqueous alteration under low-temperature conditions; however, the Murchison AOA analyzed in this study is similar in texture and elemental composition to AOAs from the unaltered meteorites.

In situ O-isotopic analyses were collected using a modified Cameca ims-1270 ion microprobe at Tokyo Institute of Technology (TiTech). A primary ion beam of mass filtered Cs^+ ions accelerated to 20 keV was used to excavate shallow pits of ~3 × 5 μm across, which, due to small sizes (typically <10 μm) of low-Ca pyroxene in AOAs, was critical in this study. The primary current was adjusted for each measurement to obtain a count rate of $^{16}O^-$ ions of ~3.5 to 4 × 10^5 cps. Each measurement consisted of 60 cycles, of 40 s each and ~10–20 min presputtering to remove the carbon coating. A normal-incident electron gun was used for charge compensation of analyzed areas. Negative secondary ions from the ^{16}O tail, ^{16}O, ^{17}O, ^{16}OH, and ^{18}O were analyzed at a mass resolution power of ~6000, sufficient to completely separate ^{16}OH interference on ^{17}O. Secondary ions were detected by an electron multiplier in pulse counting mode, and analyses were corrected for dead time. Instrumental mass fractionation was corrected using San Carlos olivine as a standard. Results are reported in per mil deviations from the standard mean ocean water (SMOW) using delta notation where $\delta^{17,18}O = [(^{17,18}O/^{16}O)_{sample}/(^{17,18}O/^{16}O)_{SMOW} - 1] \times 1000$ (Table 1; Fig. 5 ^{16}O excesses are reported in $\Delta^{17}O = \delta^{17}O - 0.52 \times \delta^{18}O$ (deviation from the terrestrial mass fractionation line of slope 0.52). Precision of individual measurements (1σ) is ~1.7‰ for $\delta^{18}O$ and ~2.5‰ for $\delta^{17}O$. Before and after oxygen isotopic measurements, each AOA analyzed was examined in back-scattered and secondary electron images to verify the locations of the sputtered craters and the mineralogy of the phases analyzed. Low-Ca pyroxene-bearing regions in AOAs analyzed for O-isotopic compositions before and after ion microprobe measurements are illustrated in Figures 1–4. Because of the small grain sizes, we failed to obtain clean spot analysis of O-isotopic composition of low-Ca pyroxene in AOA Acfer 094 #105. To resolve this problem, this AOA has been studied with the high precision isotope imaging (isotopography) by a TiTech isotope microscope system (Cameca ims-1270 + SCAPS) (Yurimoto et al., 2003). Spatial resolution of the isotopography is ~ 2 μm with precision of ~ 5‰ (1σ). Other experimental conditions were similar to those of Yurimoto et al. (2003) and Kunihiro et al. (2004).

3. RESULTS

The mineralogy and petrology of AOAs with and without low-Ca pyroxene in carbonaceous chondrites are characterized in detail in Krot et al. (2004a). Here, we briefly describe only the px-AOAs analyzed for O-isotopic compositions.

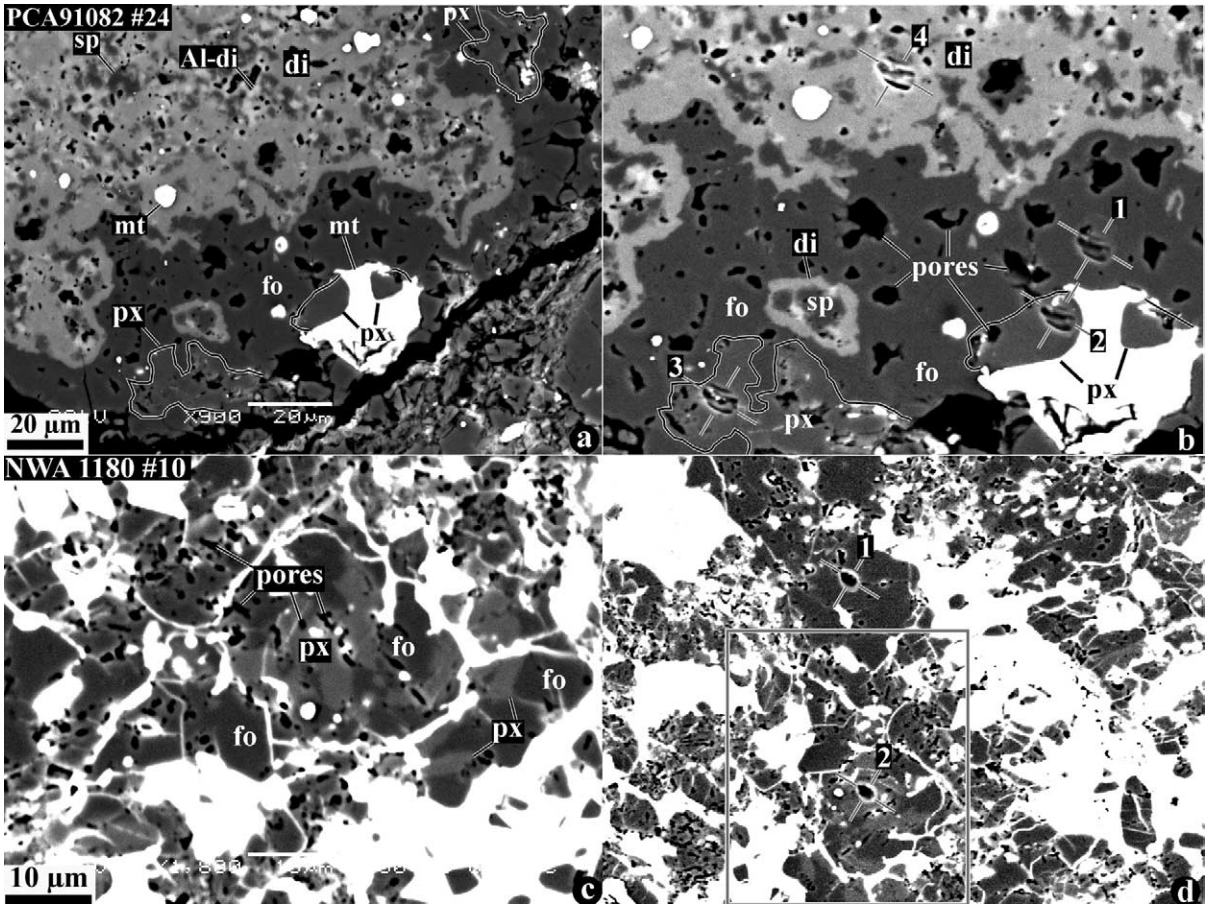

Fig. 1. BSE images of AOA #24 (a, b) and AOA #10 (c, d) in the CR carbonaceous chondrites PCA91082 and NWA 1180, respectively. (a, b) AOA #24 contains abundant CAIs surrounded by forsterite (fo); both components contain rounded inclusions of Fe,Ni-metal (mt) and preserved some porosity. The CAIs largely consist of Al-diopside (di) and spinel (sp); anorthite (an) and melilite (absent in the field of view) are minor. Low-Ca pyroxene (px; outlined in (a) and (b)) replaces forsterite along grain boundaries and around Fe,Ni-metal nodules; it also occurs as subhedral grains intergrown with Fe,Ni-metal. (c, d) AOA #10 is a porous aggregate of forsterite, CAIs (absent in the field of view) composed of anorthite and Al-diopside, and Fe,Ni-metal grains. Low-Ca pyroxene replaces forsterite along grain boundaries and around FeNi-metal nodules in the peripheral portion of the AOA. Region outlined in (d) corresponds to an area shown in (c); images in (c) and (d) are rotated relative to one another. Images "a, b" and "c, d" were taken before and after ion probe analyses respectively. Ion probe spots are labeled in (b) and (d); numbers correspond to spot numbers listed in Table 2.

3.1. Amoeboid Olivine Aggregates with ^{16}O-Enriched Low-Ca Pyroxene

AOA #24 in PCA91082 (Fig. 1a,b) is an irregularly shaped object containing ~50 vol% of CAIs surrounded by a relatively porous aggregate of forsterite ($Fa_{0.5}$, Table 1) grains; both components contain rounded inclusions of Fe,Ni-metal. The CAIs largely consist of Al-diopside and anhedral spinel grains; anorthite and melilite ($Åk_{13}$) are rare. Melilite is preferentially concentrated in the central part of the AOA, whereas anorthite is mainly present in its outer portion. Low-Ca pyroxene ($Fs_{1.6}Wo_{0.9}$; Table 1) replaces forsterite along grain boundaries and around Fe,Ni-metal nodules; it also occurs as subhedral grains intergrown with Fe,Ni-metal. Forsterite, Al-diopside, and low-Ca pyroxene intergrown with Fe,Ni-metal (spot 3, Fig. 1b) are similarly ^{16}O-enriched ($\Delta^{17}O \sim -28‰$ to $-24‰$). Low-Ca pyroxene replacing forsterite along grain boundaries and containing abundant pores (spot 2, Fig. 1b) is ^{16}O-depleted ($\Delta^{17}O \sim -13‰$), possibly due to submicron-sized inclusions of secondary minerals in pores (Table 2; Fig. 5).

AOA #10 in NWA 1180 (Fig. 1c,d) is an irregularly shaped, porous object consisting of subhedral forsterite grains ($Fa_{0.8}$, Table 1), rounded Fe,Ni-metal nodules and CAIs largely composed of anorthite and minor Al-diopside. In the outer portion of AOA, forsterite along grain boundaries and around Fe,Ni-metal nodules is replaced by low-Ca pyroxene ($Fs_{1.4}Wo_{1.4}$; Table 1). Forsterite and low-Ca pyroxene are similarly ^{16}O-enriched ($\Delta^{17}O \sim -25‰$ to $-22‰$) (Table 2; Fig. 5).

AOA #105 in Acfer 094 (Fig. 2) is an irregularly shaped, relatively porous object composed of forsterite ($Fa_{0.4}$, Table 1), rare Fe,Ni-metal grains, and numerous irregularly shaped Al-diopside-anorthite inclusions, which are uniformly distributed in central portion of the AOA and nearly absent in its rather compact outer portion. Al-diopside tends to form a layer between anorthite and forsterite. Low-Ca pyroxene ($Fs_{0.6}Wo_{0.7}$, Table 1) occurs as a 5–15 μm discontinuous layer replacing

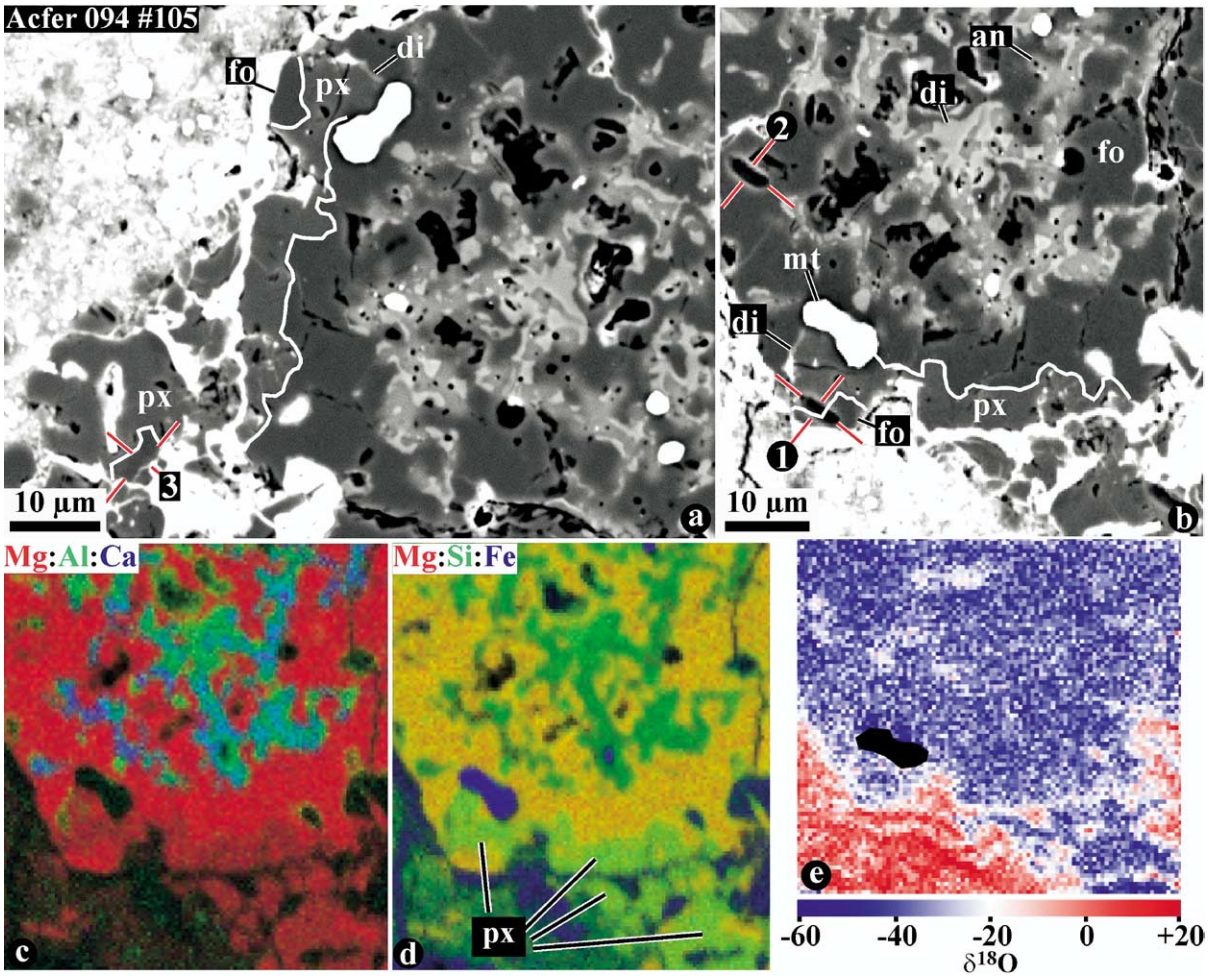

Fig. 2. BSE images (a, b), combined X-ray elemental maps (c) in Mg (red), Ca (green), and Al Kα (blue), and (d) in Mg (red), Si (green), and Fe Kα (blue), and $\delta^{18}O$ map (e) of AOA #105 in the ungrouped carbonaceous chondrite Acfer 094. The AOA consists of forsterite, rare Fe,Ni-metal grains, and numerous irregularly shaped Al-diopside-anorthite inclusions, which are uniformly distributed in the central part of the AOA and nearly absent in its outer part. Fe,Ni-metal grains are preferentially concentrated in forsterite. Low-Ca pyroxene (outlined in (a)) replaces forsterite in the outermost portion of the AOA. Images in (a) and (b) are rotated relative to one another. Ion probe spots are labeled in (a) and (b); numbers correspond to spot numbers listed in Table 2. Forsterite, anorthite, Al-diopside, and low-Ca pyroxene are similarly ^{16}O-enriched.

forsterite in the outermost portion of AOA. Although we failed to obtain a clean spot analysis of O-isotopic composition of low-Ca pyroxene, the ^{16}O-rich composition of forsterite ±low-Ca pyroxene ($\Delta^{17}O \sim -24‰$ to $-30‰$) (Table 2; Fig. 5) together with the relatively uniform distribution of $\delta^{18}O$ in the AOA obtained by isotopography (Fig. 2) suggest that low-Ca pyroxene, anorthite and Al-diopside are similarly ^{16}O-enriched.

The PCA91082 #24 and Acfer 094 #105 AOAs appear to have experienced small degrees of melting; the NWA 1180 #10 AOA shows no evidence for melting (Krot et al., 2004a).

3.2. Amoeboid Olivine Aggregates with ^{16}O-Depleted Low-Ca Pyroxene

AOA #35 in PCA91082 (Fig. 3) is an irregularly shaped, compact object composed of Cr-rich forsterite (Fa_1; Cr_2O_3, 0.84 wt%, Table 1), Fe,Ni-metal nodules, and numerous irregularly shaped Al-diopside-anorthite±spinel inclusions. Al-diopside occurs as tiny subhedral grains in anorthite (Fig. 9 in Krot et al., 2004a), suggesting that it may have crystallized from melt. The AOA is mineralogically zoned: its core is poor in Fe,Ni-metal and contains abundant CAIs. The mantle contains abundant Fe,Ni-metal nodules and only a few CAIs. The outermost portion consists of low-Ca pyroxenes (Fs_3Wo_5, Table 1) with abundant, tiny inclusions of Fe,Ni-metal. Forsterite grains are ^{16}O-rich ($\Delta^{17}O \sim -21‰$), whereas low-Ca pyroxene corroding forsterite is ^{16}O-poor ($\Delta^{17}O \sim -4‰$) (Table 2; Fig. 5).

AOA #32 in the CM chondrite Murchison is a fragmented, compact object consisting of forsterite ($Fa_{1.1}$, Table 1), rare sulfide nodules, and abundant irregularly shaped anorthite-Al-diopside inclusions (Fig. 4). The Al-diopside occurs as euhedral and subhedral inclusions in anorthite, suggesting crystallization from melt. Forsterite in the outermost portion of the AOA is corroded by Al-bearing low-Ca pyroxene (Fs_2Wo_4; 1

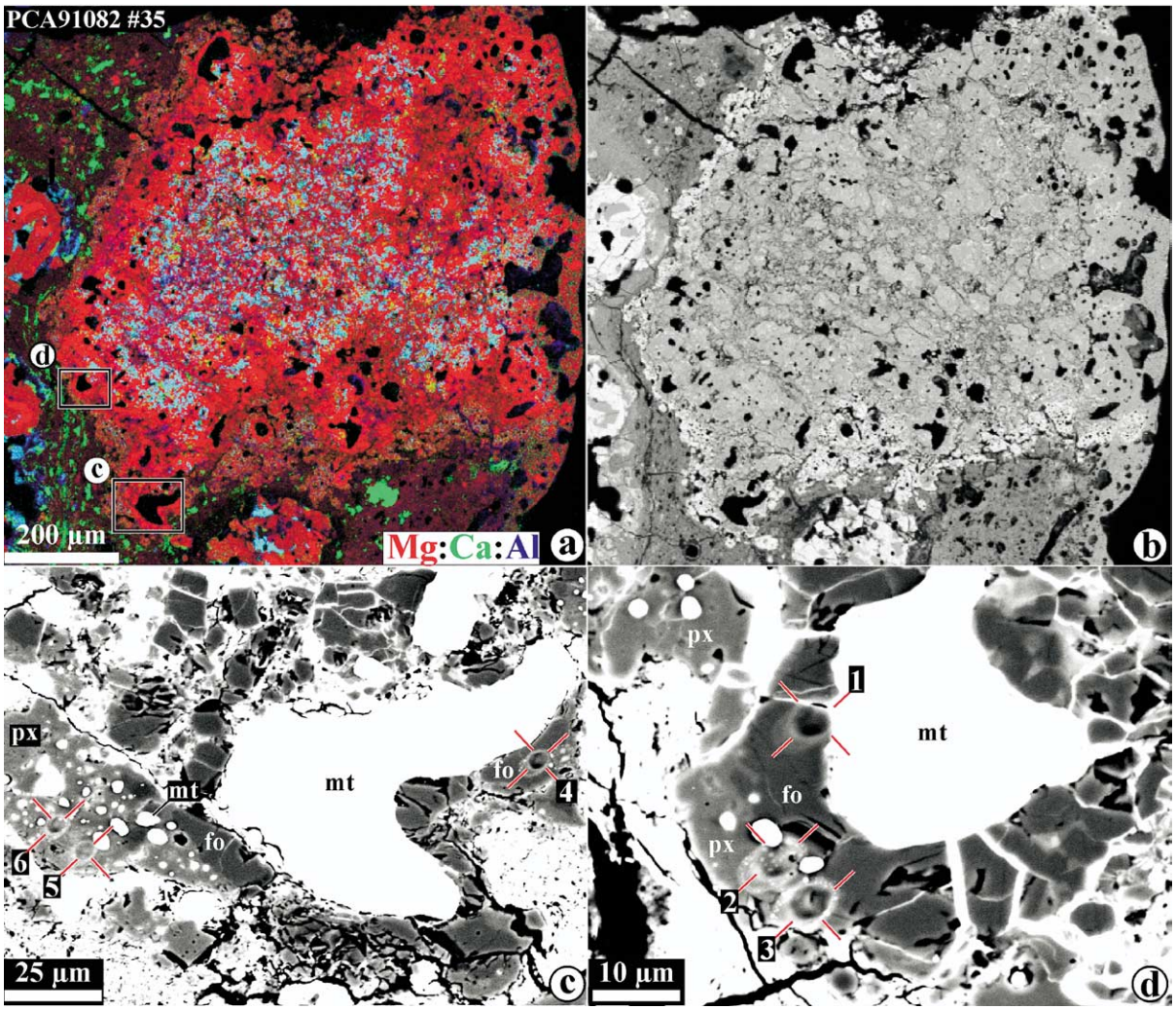

Fig. 3. Combined X-ray elemental map in Mg (red), Ca (green), and Al Kα (blue) (a), elemental map Si Kα (b), and BSE images (c, d) of AOA #35 in the CR chondrite PCA91082. The AOA consists of forsterite (red in (a)), anorthite+Al-diopside (bluish and greenish in (a)), and Fe,Ni-metal (black in (a, b)), and is mineralogically zoned. Its core is enriched in Al-diopside and anorthite and depleted in Fe,Ni-metal relative to the mantle zone. AOA is surrounded by a continuous layer of low-Ca pyroxene (white in (b)) with abundant, tiny inclusions of Fe,Ni-metal. The pyroxene replaces forsterite. Regions outlined in (a) are shown in detail in (c, d). Ion probe spots labeled in (c, d); numbers correspond to spot numbers listed in Table 2.

wt% Al_2O_3, Table 1) with abundant, tiny inclusions of Fe,Ni-metal. In some places, low-Ca pyroxene is in direct contact with anorthite that may explain high Al-content in the former. Low-Ca pyroxene also forms a thin layer around an opaque nodule. Forsterite is ^{16}O-enriched, but shows some variations in O-isotopic compositions ($\Delta^{17}O \sim -25‰$ to $-16‰$); the low-Ca pyroxene layer around AOA is ^{16}O-poor ($\Delta^{17}O \sim -6‰$) (Table 2; Fig. 5). The low-Ca pyroxene layer around the sulfide nodule is too thin for ion microprobe analysis.

The PCA91082 #35 and Murchison #32 AOAs experienced small degrees (~10%–20%) of melting, which is however larger than those of AOAs with ^{16}O-enriched low-Ca pyroxene.

3.3. AOA/Chondrule-like Object

AOA/chondrule-like object #1 from the reduced CV chondrite Leoville (Fig. EA1, Electronic Annex) consists of subhedral and euhedral forsterite grains ($Fa_{0.9-2.4}$, Table 1), abundant spinel grains, anorthitic mesostasis ($An_{95.9 \pm 2.7}$), and igneously zoned pyroxenes ranging in compositions from pigeonite (Fs_1Wo_5) to augite (Fs_1Wo_{40}). It is surrounded by an igneous rim largely composed of low-Ca pyroxene and Fe,Ni-metal nodules. Spinel is ^{16}O-rich ($\Delta^{17}O \sim -22‰$); the neighboring anorthite is ^{16}O-depleted ($\Delta^{17}O \sim -11‰$) (Table 2; Fig. 5).

4. DISCUSSION

Oxygen isotopic measurements of px-AOAs revealed the existence of ^{16}O-enriched and ^{16}O-depleted low-Ca pyroxenes, whereas forsterite is typically ^{16}O-rich (the only exception is slightly ^{16}O-depleted composition of olivine in spot 1 in the Murchison AOA #32) (Fig. 5). It is generally accepted that forsterite in AOAs formed by gas-solid condensation (e.g., Grossman and Steele, 1976; Komatsu et al.,

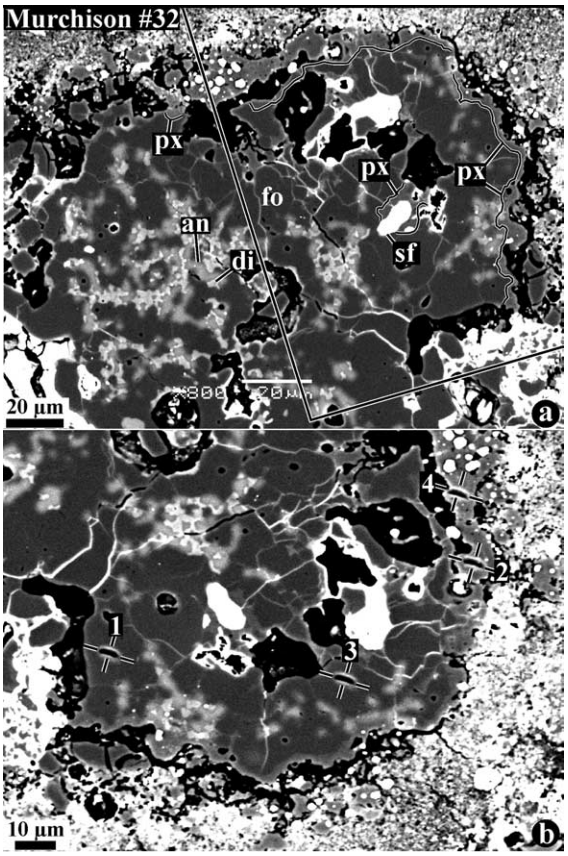

Fig. 4. BSE images of AOA #32 in the CM carbonaceous chondrite Murchison. The AOA consists of forsterite, anorthite, Al-diopside, Fe,Ni-metal and low-Ca pyroxene. Al-diopside occurs as subhedral grains in anorthite, suggesting crystallization from melt. Forsterite in the outermost portion of the AOA is corroded by low-Ca pyroxene (outlined). Region outlined in (a) is shown in (b). Images (a) and (b) were taken before and after ion probe analyses, respectively. Ion probe spots are labeled in (b) correspond to spot numbers listed in Table 2.

2001; Chizmadia et al., 2002; Itoh et al., 2002; Krot et al., 2004a):

$$2Mg_{(g)} + SiO_{(g)} + 3H_2O_{(g)} = Mg_2SiO_{4(s)} + H_{2(g)}. \quad (1)$$

The condensation origin of forsterite together with its ^{16}O-rich compositions suggests that forsterite condensed from an ^{16}O-rich gas. Variations in O-isotopic composition of olivine in AOA #32, together with petrographic evidence of its melting (Fig. 4), are probably due to incomplete oxygen isotope exchange during melting in an ^{16}O-poor gaseous reservoir. Alternatively, the ^{16}O-depleted analysis of olivine may be contaminated by submicron-sized inclusions of secondary phases below the polished surface of AOA.

Among three textural occurrences of low-Ca pyroxene reported by Krot et al. (2004a), the thin discontinuous layers around forsterite grains or along forsterite grain boundaries as well as the haloes and subhedral grains around Fe,Ni-metal nodules in AOA peripheries (Figs. 1, 2) have ^{16}O-rich compositions. The porous textures of the AOAs containing ^{16}O-rich low-Ca pyroxene and the mineralogical observations indicating that these low-Ca pyroxenes formed by a reaction between forsterite and gaseous SiO[1]:

$$Mg_2SiO_{4(s)} + SiO_{(g)} + H_2O_{(g)} = Mg_2Si_2O_{6(s)} + H_{2(g)} \quad (2)$$

suggest that ^{16}O-rich low-Ca pyroxenes formed in the same, ^{16}O-rich gaseous reservoir as forsterite of their host AOAs, but at lower temperatures.

Based on the mineralogical studies of AOAs and a thermodynamic analysis, Krot et al. (2004c) inferred other condensation reactions recorded by CAIs in AOAs, which must have occurred at higher temperatures, before condensation of forsterite and low-Ca pyroxene. These include replacement of melilite by Al-diopside, spinel, and anorthite:

$$Ca_2Al_2SiO_{7(s)} + 3SiO_{(g)} + 3Mg_{(g)} + 6H_2O_{(g)} = 2CaMgSi_2O_{6(s)} + MgAl_2O_{4(s)} + 6H_{2(g)} \quad (3)$$

$$Ca_2Al_2SiO_{7(s)} + 3SiO_{(g)} + Mg_{(g)} + 4H_2O_{(g)} = CaAl_2Si_2O_{8(s)} + CaMgSi_2O_{6(s)} + 4H_{2(g)} \quad (4)$$

replacement of spinel by Al-diopside and anorthite

$$2MgAl_2O_{4(s)} + 2CaMgSi_2O_{6(s)} + SiO_{(g)} + H_2O_{(g)} = CaAl_2Si_2O_{8(s)} + 2Mg_2SiO_{4(s)} + CaAl_2SiO_{6(s)} + H_{2(g)} \quad (5)$$

and enrichment of diopside in Al

$$3Ca_2Al_2SiO_7 + MgAl_2O_4 + 5SiO_{(g)} + Mg_{(g)} + 6H_2O_{(g)} = [4CaAl_2SiO_6 + 2CaMgSi_2O_6]_{(px\ ss)} + 6H_{2(g)}. \quad (6)$$

These observations and the ^{16}O-rich compositions of spinel, anorthite, and Al-diopside in AOAs from primitive carbonaceous chondrites (e.g., Hiyagon and Hashimoto, 1999a,b; Krot et al., 2001; Aléon et al., 2002a; Itoh et al., 2002; Fagan et al., 2004; this study) suggest that these reactions also occurred in the ^{16}O-rich gaseous reservoir. During these series of reactions small amounts of melts in the host AOAs may have existed as well. Based on these observations and the ^{16}O-rich isotopic compositions of the more refractory solar nebula condensates, such as corundum, hibonite, grossite, spinel, and melilite (e.g., Aléon et al., 2002a,b; Simon et al., 2002; Huss et al., 2003), we infer that the ^{16}O-rich gaseous reservoir (Krot et al., 2002a) was dominant through out the entire condensation temperature range recorded by CAIs and AOAs (i.e., from corundum to low-Ca pyroxene). Whether this reservoir was localized (e.g., McKeegan et al., 1998; Scott and Krot, 2001) or occupied initially the entire inner solar nebula (Yurimoto and Kuramoto, 2002; Kobayashi et al., 2003; Clayton, 2004; Lyons and Young, 2004; Krot et al., 2005) remains unknown.

Low-Ca pyroxenes with ^{16}O-poor compositions are observed as shells of variable thickness, commonly with abundant, tiny inclusions of Fe,Ni-metal grains, around AOAs having compact textures (Figs. 3, 4). This textural occurrence of low-Ca pyroxene suggests that the ^{16}O-poor low-Ca pyroxenes formed by melting of the pyroxene-normative dust deposited on the

[1] Krot et al. (2003a) considered another reaction for the origin of low-Ca pyroxene around Fe,Ni-metal nodules, $Mg_2SiO_4 + Si_{(in\ FeNi)} + 2H_2O_{(g)} = Mg_2Si_2O_6 + 2H_{2(g)}$, but concluded that it was unimportant.

Table 2. Ion microprobe analyses of oxygen isotopic compositions of individual minerals in AOAs and AOA/chondrule-like objects.[a]

Chondrite	Class	Object	No.	Mineral	Spot no.	$\delta^{17}O$	1σ	$\delta^{18}O$	1σ	$\Delta^{17}O$	1σ
PCA91082	CR	AOA	35	fo	1	−41.8	2.6	−37.1	1.9	−22.4	2.8
PCA91082	CR	AOA	35	fo	4	−39.5	1.9	−36.1	1.4	−20.7	2.1
PCA91082	CR	AOA	35	px	2	−1.4	2.9	3.9	1.6	−3.5	3.0
PCA91082	CR	AOA	35	px	3	−1.1	2.8	5.3	1.8	−3.9	2.9
PCA91082	CR	AOA	35	px	5	−0.8	2.2	5.6	1.8	−3.7	2.4
PCA91082	CR	AOA	35	px	6	−1.9	2.0	5.8	1.4	−4.9	2.1
PCA91082	CR	AOA	24	fo	1	−44.9	2.6	−41.0	2.1	−23.6	2.8
PCA91082	CR	AOA	24	px	2	−50.8	2.8	−44.2	2.2	−27.8	3.0
PCA91082	CR	AOA	24	px	3	−34.0	3.4	−40.0	3.0	−13.3	3.8
PCA91082	CR	AOA	24	di	4	−49.9	3.5	−43.9	2.9	−27.1	3.8
NWA 1180	CR	AOA	10	fo	1	−52.8	2.8	−53.7	2.2	−24.8	3.1
NWA 1180	CR	AOA	10	px	2	−51.3	2.7	−56.7	1.5	−21.8	2.9
Acfer 094	ungr.	AOA	105	fo + px	1	−49.1	2.6	−48.4	2.3	−24.0	2.9
Acfer 094	ungr.	AOA	105	fo	2	−56.4	2.4	−50.0	1.8	−30.4	2.6
Acfer 094	ungr.	AOA	105	fo	3	−51.0	2.5	−50.5	1.7	−24.7	2.7
Murchison	CM	AOA	32	fo	1	−34.1	3.9	−35.3	3.6	−15.7	4.3
Murchison	CM	AOA	32	fo	3	−50.9	3.3	−49.8	1.9	−25.0	3.4
Murchison	CM	AOA	32	px + fo	2	−24.5	2.8	−22.4	2.2	−12.9	3.0
Murchison	CM	AOA	32	px	4	−10.4	3.0	−7.5	2.5	−6.5	3.2
Leoville	CV	AOA/chd	1	sp	1	−47.9	2.5	−50.5	1.6	−21.7	2.6
Leoville	CV	AOA/chd	1	pl	2	−12.2	3.2	−2.1	3.0	−11.1	3.6

[a] di = Al-diopside; fo = forsterite; pl = anorthitic plagioclase; px = low-Ca pyroxene; sp = spinel; class = classification.

surface of the host AOAs. This is supported by the presence of subhedral and euhedral grains of Al-diopside in anorthite in the AOAs #35 and #32 and by the direct contact between low-Ca pyroxene shell and anorthite in the latter (Figs. 3, 4). An igneous origin of the ^{16}O-poor low-Ca pyroxenes could also explain the high contents of the refractory lithophile elements, such as CaO, Al_2O_3 and TiO_2, in the pyroxenes (Table 1); these elements are not expected to be in the gaseous phase at the condensation temperatures of low-Ca pyroxene. In addition, these pyroxenes have higher FeO contents (Fs_{2-3}) than those in forsterites ($Fa_{\sim 1}$) of their host AOAs, suggesting formation at different redox conditions. Possible formation mechanisms of the pyroxene-normative dust are discussed below.

Direct condensation of low-Ca pyroxene [i.e., $Mg_{(g)} + SiO(g) + 2H_2O_{(g)} = MgSiO_3 + 2H_{2(g)}$] is not predicted from a gas of solar composition under equilibrium conditions (Yoneda and Grossman, 1995; Petaev and Wood, 1998; Ebel and Grossman, 2000; Ebel et al., 2003), but could have occurred from a fractionated (Mg/Si < solar) gas. Such gas could have been produced by an isolation of forsterite from the cooling nebular gas (Petaev and Wood, 1998; Ebel et al., 2003) or by repeated evaporation-recondensation processes due to higher volatility of Si compared to Mg (Nagahara and Ozawa, 2003). The existence of fractionated nebular gas in chondrule-forming region(s) has been inferred to explain (*i*) the chemical compositions of Fe,Ni-metal in the matrix and chondrule rims in CR chondrites (Connolly et al., 2001), (*ii*) the layered structures (olivine-rich core → pyroxene-rich mantle → silica-rich igneous rim) of Type I chondrules in CR chondrites (Krot et al., 2000), (*iii*) the complementary compositions of the CR chondrules and matrices (Palme and Klerner, 2000), and (*iv*) the origin of pyroxene-rich and olivine-rich chondrules in ordinary chondrites (Tachibana et al., 2003). Finally, it is generally accepted that an ^{16}O-poor gaseous reservoir existed in chondrule-forming region(s) (e.g., Leshin et al., 2000; Krot et al., 2005).

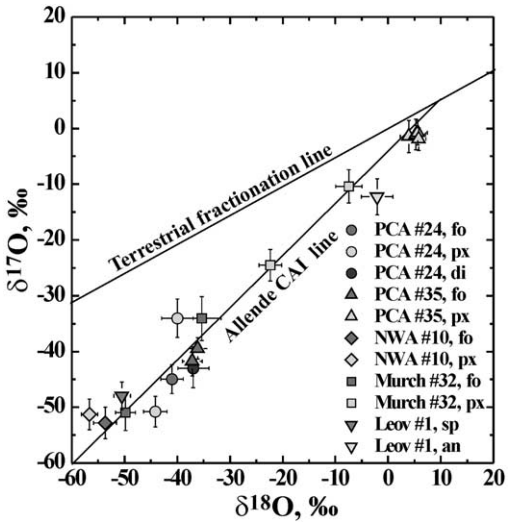

Fig. 5. Oxygen isotopic compositions of AOAs with low-Ca pyroxene and AOA/Al-rich chondrule-like object in the PCA91082 (PCA), NWA 1180 (NWA), Murchison (Murch) and Leoville (Leov) chondrites (error bars are 1σ). Terrestrial fractionation line and Allende CAI line are shown for reference. Forsterite grains in AOAs are ^{16}O-rich; low-Ca pyroxenes show ^{16}O-rich and ^{16}O-poor compositions. Spinel in the Leoville AOA/chondrule-like object is ^{16}O-rich; anorthitic plagioclase is ^{16}O-poor. an = anorthitic plagioclase; di = Al-diopside; fo = forsterite; px = low-Ca pyroxene; sp = spinel.

Based on these observations, we infer that ^{16}O-poor low-Ca pyroxenes in AOAs probably formed in chondrule-forming region(s). If this interpretation is correct, it implies at least some of the AOAs formed before chondrules and were subsequently thermally processed together with chondrules. This interpretation is consistent with the presence of the ^{16}O-rich, relict forsterite grains in magnesian chondrules (e.g., Itoh et al., 2002; Jones, 2002; Choi et al., 2003; Jones et al., 2004) and their igneous rims (Nagashima et al., 2003), and of the ^{16}O-rich ferrous olivine in Type II chondrule (Yurimoto and Wasson, 2002). It is also supported by the AOA/chondrule-like object in Leoville, which, underwent substantial melting and yet preserved some textural and mineralogical resemblance to AOAs (Krot et al., 2004a) and its original ^{16}O-rich signature in the unmelted spinel grains (Table 2; Figs. 5, EA1). The ^{16}O-depleted compositions of igneous plagioclase in this object suggest that the melting probably accompanied by O-isotopic exchange. Oxygen isotopic exchange during melting of ^{16}O-rich precursors has been previously inferred for some CAIs in CV and CR chondrites (Yurimoto et al., 1998; Aléon et al., 2002), although no connection to chondrule formation has been proposed. The latter has been recently suggested based on a correlated study of oxygen and ^{26}Al-^{26}Mg isotopic systematics of igneous CAIs in CR chondrites (Hutcheon et al., 2004; Krot et al., 2005).

Based on the mineralogy and bulk chemistry of AOAs and magnesian chondrules, it was concluded that chondrules cannot be produced from AOAs by an igneous fractionation; addition of silica-rich material enriched in moderately volatile elements, such as Mn, Cr, and Na, to AOAs is required (e.g., Komatsu et al., 2001; Krot and Keil, 2002; Krot et al., 2002b, 2004a,b; MacPherson and Huss, 2005). The presence of AOAs with ^{16}O-depleted low-Ca pyroxene shells and AOA/chondrule-like objects provides the evidence for transformation of refractory inclusions into chondrules, which must have been accompanied by O-isotopic exchange between melted ^{16}O-rich precursor materials and ^{16}O-poor gaseous reservoir.

5. CONCLUSIONS

Amoeboid olivine aggregates (AOAs) in primitive carbonaceous chondrites consist of forsterite ($Fa_{<2}$), Fe,Ni-metal, spinel, Al-diopside, anorthite, and rare gehlenitic melilite ($Åk_{<15}$). ~10% of AOAs contain low-Ca pyroxene ($Fs_{1–3}Wo_{1–5}$) that is in corrosion relationship with forsterite and is found in three major textural occurrences: (*i*) thin (<15 μm) discontinuous layers around forsterite grains or along forsterite grain boundaries in AOA peripheries; (*ii*) 5–10-μm-thick haloes and subhedral grains around Fe,Ni-metal nodules in AOA peripheries, and (*iii*) shells of variable thickness (up to 70 μm), commonly with abundant tiny (3–5 μm) inclusions of Fe,Ni-metal grains, around AOAs. AOAs with the low-Ca pyroxene shells are compact and appear to have experienced small (10%–20%) degree of melting. AOAs with other textural occurrences of low-Ca pyroxene are rather porous. Forsterite grains in AOAs with low-Ca pyroxene have typically ^{16}O-rich isotopic compositions ($\Delta^{17}O < -20‰$). Low-Ca pyroxenes of textural occurrences (*i*) and (*ii*) are similarly ^{16}O-enriched, whereas those of (*iii*) are ^{16}O-depleted ($\Delta^{17}O \sim -6‰$ to $-4‰$).

We conclude that AOAs are aggregates of solar nebular condensates that originated in an ^{16}O-rich gaseous reservoir, probably the CAI-forming region(s). Forsterites in some AOAs reacted with gaseous SiO in the same nebular region to form low-Ca pyroxene. Some other AOAs appear to have accreted ^{16}O-poor pyroxene-normative dust and experienced varying degrees of melting, most likely in chondrule-forming region(s). (Krot et al., 2003c; Grossman et al. 1979; Krot et al., 2004c; Imae et al., 1993)

Acknowledgments—We thank H. C. Connolly Jr., A. M. Davis, and S. S. Russell for the constructive reviews. This work was supported by NASA grants NAG5-10610 (A. N. Krot, P.I.), NAG5-11591 (K. Keil, P.I.), NAG5-10484 (S. B. Jacobsen, P.I.), and Monkasho grants (H. Yurimoto, P.I.). This is Hawaii Institute of Geophysics and Planetology publication No. 1371 and School of Ocean and Earth Science and Technology publication No. 6543.

Associate editor: S. Russell

REFERENCES

Aléon J., Krot A. N., and McKeegan K. D. (2002a) Ca-Al–rich inclusions and amoeboid olivine aggregates from the CR carbonaceous chondrites. *Meteorit. Planet. Sci.* **37,** 1729–1755.

Aléon J., Krot A. N., McKeegan K. D., MacPherson G. J., and Ulyanov A. A. (2002b) Oxygen isotopic composition of fine-grained Ca-Al–rich inclusions in the reduced CV3 chondrite Efremovka. *Lunar Planet. Sci.* **33,** 1426.

Chizmadia L. J., Rubin A. E., and Wasson J. T. (2002) Mineralogy and petrology of amoeboid olivine inclusions in CO3 chondrites: Relationship to parent-body aqueous alteration. *Meteorit. Planet. Sci.* **37,** 1781–1796.

Choi B.-G., Park S., and Yurimoto H. (2003) Extreme oxygen isotope heterogeneity in a chondrule olivine phenocryst (abstract). *Meteorit. Planet. Sci.* **38** (*Suppl.*), A50.

Clayton R. N. (2004) Solar ^{18}O/^{17}O and the setting for solar birth. *Lunar Planet. Sci.* **35,** 1045.

Connolly H. C. Jr., Huss G. R., and Wasserburg G. J. (2001) On the formation of Fe-Ni metal in Renazzo-like carbonaceous chondrites. *Geochim. Cosmochim. Acta* **65,** 4567–4588.

Cohen R. E., Kornacki A. L., and Wood J. A. (1983) Mineralogy and petrology of chondrites and inclusions in the Mokoia CV3 chondrite. *Geochim. Cosmochim. Acta* **47,** 1739–1757.

Ebel D. S. and Grossman L. (2000) Condensation in dust-enriched systems. *Geochim. Cosmochim. Acta* **64,** 339–366.

Ebel D. S., Engler A., and Kurat G. (2003) Pyroxene chondrules from olivine-poor dust-enriched systems (abstract). *Lunar Planet. Sci.* **34,** 2059.

Fagan T. J., Krot A. N., Keil K., and Yurimoto H. (2004) Oxygen isotopic compositions of amoeboid olivine aggregates in the reduced CV3 chondrites Efremovka, Vigarano and Leoville. *Geochim. Cosmochim. Acta* **68,** 2405–2611.

Grossman L. and Steele I. M. (1976) Amoeboid olivine aggregates in the Allende meteorite. *Geochim. Cosmochim. Acta* **40,** 149–155.

Hashimoto A. and Grossman L. (1987) Alteration of Al-rich inclusions inside amoeboid olivine aggregates in the Allende meteorite. *Geochim. Cosmochim. Acta* **51,** 1685–1704.

Hiyagon H. and Hashimoto A. (1999a) ^{16}O excesses in olivine inclusions in Yamato-86009 and Murchison chondrites and their relation to CAIs. *Science* **283,** 828–831.

Hiyagon H. and Hashimoto A. (1999b) An ion microprobe study of oxygen isotopes in various types of inclusions in Y-82050 (CO3), ALHA77307 (CO3) and Y-86009 (CV3) chondrites (abstract). *Lunar Planet. Sci.* **30,** 1319.

Huss G. R., Hutcheon I. D., Krot A. N., and Tachibana S. (2003) Oxygen isotopes in refractory inclusions from the Adelaide carbonaceous chondrite (abstract). *Lunar Planet. Sci.* **34,** 1802.

Hutcheon I. D., Krot A. N., Marhas K., and Goswami J. (2004) Magnesium isotopic compositions of igneous CAIs in the CR

carbonaceous chondrites: Evidence for an early and late-stage melting of CAIs (abstract). *Lunar Planet. Sci.* **35,** 2124.

Itoh S., Rubin A. E., Kojima H., Wasson J. T., and Yurimoto H. (2002) Amoeboid olivine aggregates and AOA-bearing chondrule from Y-81020 CO 3.0 chondrite: Distribution of oxygen and magnesium isotopes (abstract). *Lunar Planet. Sci.* **33,** 1490.

Jones R. H. (2002) Heterogeneities in the oxygen isotope ratios of chondrules and their significance for models of the early solar system (abstract). *Meteorit. Planet. Sci.* **37** (*Suppl.*), A73.

Jones R. H., Leshin L. A., Guan Y., Sharp L. A., Durakiewics T., and Schilk A. J. (2004) Oxygen isotope heterogeneity in chondrules from the Mokoia carbonaceous chondrite. *Geochim. Cosmochim. Acta*, 68, 3423-3438.

Kobayashi S., Imai H., and Yurimoto H. (2003) New extreme ^{16}O-rich reservoir in the early solar system. *Geochem. J.* **37,** 663–669.

Komatsu M., Krot A. N., Petaev M. I., Ulyanov A. A., Keil K., and Miyamoto M. (2001) Mineralogy and petrography of amoeboid olivine aggregates from the reduced CV3 chondrites Efremovka, Leoville and Vigarano: Products of nebular condensation and accretion. *Meteorit. Planet. Sci.* **36,** 629–643.

Kornacki A. S. and Wood J. A. (1984a) Petrography and classification of Ca,Al-rich and olivine-rich inclusions in the Allende CV3 chondrite. *J. Geophys. Res.* **89,** B573–B587.

Kornacki A. S. and Wood J. A. (1984b) The mineral chemistry and origin of inclusion matrix and meteorite matrix in the Allende CV3 chondrite. *Geochim. Cosmochim. Acta* **48,** 1663–1676.

Krot A. N., Weisberg M. K., Petaev M. I., Keil K., and Scott E. R. D. (2000) High-temperature condensation signatures in Type I chondrules from CR carbonaceous chondrites (abstract). *Lunar Planet. Sci.* **31,** 1470.

Krot A. N., McKeegan K. D., Russell S. S., Meibom A., Weisberg M. K., Zipfel J., Krot T. V., Fagan T. J., and Keil K. (2001) Refractory Ca,Al-rich inclusions and Al-diopside–rich chondrules in the metal-rich chondrites Hammadah al Hamra 237 and QUE 94411. *Meteorit. Planet. Sci.* **36,** 1189–1217.

Krot A. N. and Keil K. (2002) Anorthite-rich chondrules in CR and CH carbonaceous chondrites: Genetic link between Ca,Al-rich inclusions and ferromagnesian chondrules. *Meteorit. Planet. Sci.* **37,** 91–111.

Krot A. N., McKeegan K. D., Leshin L. A., MacPherson G. J., and Scott E. R. D. (2002a) Existence of an ^{16}O-rich gaseous reservoir in the solar nebula. *Science* **295,** 1051–1054.

Krot A. N., Hutcheon I. D., and Keil K. (2002b) Anorthite-rich chondrules in the reduced CV chondrites: Evidence for complex formation history and genetic links between CAIs and ferromagnesian chondrules. *Meteorit. Planet. Sci.* **37,** 155–182.

Krot A. N., Petaev M. I., Russell S. S., Itoh S., Fagan T. J., Yurimoto H., and Keil K. (2003c) Amoeboid olivine aggregates in primitive carbonaceous chondrites: Records of high-temperature nebular processing (abstract). *Meteorit. Planet. Sci.* **38** (*Suppl.*), A74.

Krot A. N., Petaev M. I., and Yurimoto H. (2004a) Amoeboid olivine aggregates with low-Ca pyroxenes: A genetic link between refractory inclusions and chondrules? *Geochim. Cosmochim. Acta* **68,** 1923–1941.

Krot A. N., Petaev M. I., Fagan T. J., and Yurimoto H. (2004b) Ca,Al-rich inclusions, amoeboid olivine aggregates and Al-rich chondrules from the unique carbonaceous chondrite Acfer 094: I. Mineralogy and petrology. *Geochim. Cosmochim. Acta* **68,** 2167–2184.

Krot A. N., Petaev M. I., Russell S. S., Itoh S., Fagan T., Yurimoto H., Chizmadia L., Weisberg M. K., Komatsu M., Ulyanov A. A., and Keil K. (2004c) Amoeboid olivine aggregates in carbonaceous chondrites: Records of nebular and asteroidal processes. (Invited review). *Chem. Erde* **64,** 185–239.

Krot A. N., Hutcheon I. D., Yurimoto H., Cuzzi J. N., McKeegan K. D., Scott E. R. D., Libourel G., Chaussidon M., Aléon J., and Petaev M. I. (2005) Evolution of oxygen isotopic composition in the inner solar nebula. *Astrophys. J.* (in press).

Kunihiro T., Nagashima K., and Yurimoto H. (2002) Distribution of oxygen isotopes in matrix from the Vigarano CV3 meteorite (abstract). *Lunar Planet. Sci.* XXXIII, Lunar Planet. Inst., Houston, CD-ROM #1549.

Leshin L. A., McKeegan K. D., and Benedix G. K. (2000) Oxygen isotope geochemistry of olivine from carbonaceous chondrites (abstract). *Lunar Planet. Sci.* **31,** 1918.

Lyons J. R. and Young E. D. (2004) Evolution of oxygen isotopes in the solar nebula (abstract). *Lunar Planet. Sci.* **35,** 1970.

McKeegan K. D., Leshin L. A., Russell S. S., and MacPherson G. J. (1998) Oxygen isotopic abundances in calcium-aluminum-rich inclusions from ordinary chondrites: Implications for nebular heterogeneity. *Science* **280,** 414–418.

MacPherson G. J. and Huss G. R. (2005) Petrogenesis of Al-rich chondrules: Evidence from bulk compositions and phase equilibria. *Geochim. Cosmochim. Acta* (in press).

McSween H. Y. Jr. (1977) Chemical and petrographic constraints on the origin of chondrules and inclusions in carbonaceous chondrites. *Geochim. Cosmochim. Acta* **41,** 1843–1860.

Nagahara H. and Ozawa K. (2003) Was the diversity of chondrule compositions achieved by evaporation and condensation processes? (abstract) *Meteorit. Planet. Sci.* **38** (*Suppl.*), A125.

Nagashima K., Takeda Y., Itoh S., and Yurimoto S. (2003) ^{16}O-rich olivine in igneous rim of Type I chondrule from CR2 chondrite (abstract). *Meteorit. Planet. Sci.* **38** (*Suppl.*), A77.

Palme H. and Klerner S. (2000) Formation of chondrules and matrix in carbonaceous chondrites (abstract). *Meteorit. Planet. Sci.* **35** (*Suppl.*), A124.

Petaev M. I. and Wood J. A. (1998) The condensation with partial isolation (CWPI) model of condensation in the solar nebula. *Meteorit. Planet. Sci.* **33,** 1123–1137.

Scott E. R. D. and Krot A. N. (2001) Oxygen isotopic compositions and origins of Ca-Al–rich inclusions and chondrules. *Meteorit. Planet. Sci.* **36,** 1307–1319.

Simon S. B., Davis A. M., Grossman L., and McKeegan K. D. (2002) A hibonite-corundum inclusion from Murchison: A first generation condensate from the solar nebula. *Meteorit. Planet. Sci.* **37,** 533–548.

Tachibana S., Nagahara H., Mostefaovi S. and Kita N. T. (2003) Correlation between relative ages in inferred from ^{26}Al and bulk compositions of ferromagnesian chrondules in least equilibrated ordinary chondrites. *Meteorit. Planet. Sci.* **38,** 939–962.

Yoneda S. and Grossman L. (1995) Condensation of CaO-MgO-Al_2O_3-SiO_2 liquids from cosmic gases. *Geochim. Cosmochim. Acta* **59,** 3413–3444.

Yurimoto H., Ito M., and Nagasawa H. (1998) Oxygen isotope exchange between refractory inclusion in Allende and solar nebula gas. *Science* **282,** 1874–1877.

Yurimoto H. and Kuramoto K. (2002) A possible scenario introducing heterogeneous oxygen isotopic distribution in protoplanetary disk (abstract). *Meteorit. Planet. Sci.* **37,** A153.

Yurimoto H. and Wasson J. T. (2002) Extremely rapid cooling of a carbonaceous-chondrite chondrule containing very ^{16}O-rich olivine and a ^{26}Mg excess. *Geochim. Cosmochim. Acta* **66,** 4355–4363.

Yurimoto H., Nagashima K., and Kunihiro T. (2003) High precision isotope micro-imaging of materials. *Appl. Surf. Sci.* **203–204**, 793–797.

Yurimoto H. and Kuramoto K. (2004) Molecular cloud origin for the oxygen isotope heterogeneity in the solar system. *Science* **305,** 1763–1766.

ELECTRONIC ANNEX

Supplementary data associated with this article can be found, in the online version, at 10.1016/j.gca.2004.06.046.